Membrane mimetic thermal proteome profiling (MM-TPP) towards mapping membrane protein-ligand dynamics

Rupinder Singh Jandu[1], Mohammed Al-Seragi[1], Hiroyuki Aoki[2], Mohan Babu[2], Franck Duong van Hoa[1]*

[1] Department of Biochemistry and Molecular Biology, Life Sciences Institute, University of British Columbia, Vancouver, British Columbia, Canada.
[2] Department of Biochemistry, University of Regina, Regina, Saskatchewan, Canada.
*Correspondence to: fduong@mail.ubc.ca

Abstract

Integral membrane proteins (IMPs) remain the principal target of small-molecule therapeutics, and yet modalities towards probing on and off-target hits against this protein class in a robust, unbiased, and detergent-free manner remain starkly underdeveloped. Previously, we introduced the Peptidisc membrane mimetic (MM) for the water-soluble stabilization of the *Escherichia coli* membrane proteome and interactome (Carlson et al., 2019). Herein, we implement the Peptidisc into thermal proteome profiling (TPP), enabling for the first time a broad-scale level characterization of membrane protein-ligand interactions while completely circumventing structural perturbations invoked by detergents. Using a library prepared from the whole mouse liver, we determine the influence of ATP and orthovanadate on the thermal stability of IMPs, including pharmaceutically relevant ATP-binding cassette ABC transporters and G-protein coupled receptors. MM-TPP also detects thermal stability changes driven by ATP by-products, where non-canonical ATP binders can be validated with next-generation computational tools. MM-TPP thus offers a robust platform for identifying on- and off-target ligand effects, providing insights into the druggable membrane proteome and its stability as a consequence of changing and often dynamic small molecules.

Introduction

Integral membrane proteins (IMPs) are essential to numerous cellular functions, including signal transduction, cell-cell recognition, and the transport of nutrients and ions across cellular membranes (Boulos et al., 2023). Although comprising only 20 to 30% of the human genome, they represent nearly two-thirds of druggable targets due to their significant impact on cellular physiology and their exposure to the cell surface. This prevalence highlights the critical nature of IMPs in pharmacology (Bakheet and Doig, 2009; Fagerberg et al., 2010; Helbig et al., 2010; Santos et al., 2017). However, studying the interactions between small molecule drugs and membrane proteins poses unique challenges, primarily due to the low abundance and hydrophobic characteristics of these proteins, which complicates their characterization and analysis.

Proteomics-based technologies have emerged as powerful tools for identifying protein-ligand interactions (Aebersold and Mann, 2016; Li et al., 2016). Among the methods employed, affinity purification mass spectrometry (AP-MS) (Dunham et al., 2012; Kawatani and Osada, 2014)) stands out by utilizing chemical compounds covalently attached to an affinity matrix to capture target proteins, enabling detailed characterization of their interactions. Similarly, drug affinity responsive target stability (DARTS) (Lomenick et al., 2009; Pai et al., 2015) exploits ligand-induced conformational changes through limited proteolysis, providing insights into the dynamic nature of protein interactions with ligands. On the other hand, thermal proteome profiling (TPP), originating from the cellular thermal shift assay, allows for the detection of broad ligand-induced conformation changes in proteins subjected to heat stress (Molina et al., 2013; Savitski et al., 2014). Although TPP is favored in drug screening campaigns due to its

straightforward implementation, it primarily relies on cytosolic extracts, often neglecting pharmaceutical-relevant transmembrane proteins (Franken et al., 2015; Mateus et al., 2020). Strategies to improve membrane proteome coverage, such as solubilization with detergents, have been explored (Huber et al., 2015; Kalxdorf et al., 2021; Reinhard et al., 2015); however, it is widely acknowledged that even mild detergents can disrupt protein structures and activities, leading to challenges in accurately identifying drug targets (Berlin et al., 2023; Yang et al., 2014; Ye et al., 2023).

Different membrane mimetics (MMs) have been developed over the years to maintain membrane proteins in a water-soluble state (Denisov and Sligar, 2016; Dörr et al., 2014; Young, 2023). Among them, peptidisc has emerged as a self-assembling scaffold characterized by its "one size fits all" property, effectively stabilizing integral membrane proteins (IMPs) of varying sizes and topologies (Carlson et al., 2018). This versatility has facilitated the isolation of the entire membrane proteome from bacterial to mammalian sources, collectively referred to as peptidisc libraries (Antony et al., 2024; Carlson et al., 2019; Zhao et al., 2023). These libraries are instrumental in capturing and stabilizing IMPs in their functional states while preserving their interactomes and lipid allosteric modulators, thus enabling a more comprehensive analysis of membrane dynamics and ligand interactions (Angiulli et al., 2020; Carlson et al., 2019; Jandu et al., 2024; Urner et al., 2022).

In this work, we integrate the peptidisc into the Thermal Proteome Profiling (TPP) workflow, presenting a straightforward approach for surveying IMPs-ligand interactions on a broad scale without biases typically introduced by detergents. We apply the MM-TPP method to

E. coli and mouse liver membranes, effectively assessing its capability to detect ATP binders, including ABC transporters, G protein-coupled receptors (GPCRs), and multi-subunit complexes. This innovative approach proves sensitive enough to reveal interactions mediated by ATP by-products, thereby providing critical insights into the dynamics of both system and ligand dynamics that are critical aspects to account for during small-molecule drug development.

Results

The MM-TPP workflow is illustrated in **Figure 1**. Initially, the detergent-solubilized membrane fraction is reconstituted into peptidisc libraries as detailed in previous studies (Antony et al., 2024; Carlson et al., 2019; Zhao et al., 2023). The library is subsequently divided into two aliquots, with one exposed to the ligand of interest (treatment) and the other treated with ddH_2O (control). Following this, the samples undergo heating for three minutes to facilitate protein denaturation and precipitation. The soluble fraction is then isolated through ultracentrifugation before analysis by liquid chromatography and tandem mass spectrometry (LC-MS/MS). Proteins that exhibit significant stabilization or destabilization are identified following the methodology outlined by Zhang et al. (2020), where proteins meeting the defined fold difference thresholds between triplicate treatment and control groups are considered highly probable ligand binders.

As a validation step, we determined the thermal stability of the purified and peptidisc reconstituted bacterial ABC transporter MsbA in the presence of ATP and vanadate (VO_4). Vanadate is a potent inhibitor of the ABC transporter family and upon binding with ATP, this molecule blocks the transporter in a specific conformation (Lyu et al., 2022). Accordingly, the SDS-PAGE analysis reported an increased thermal stability of MsbA in the presence of these

ligands **(Figure 2A** and **Supplementary Figure 1)**. Additional examinations involved an assessment of the ATP-VO_4 effect on a peptidisc library derived from wild-type *E. coli*, where MsbA is present at native expression levels (**Figure 2B**). Results revealed that ATP-VO_4 significantly stabilizes MsbA at temperatures of 51°C and higher (**Figure 2C**). Notably, at 61°C, the volcano plot indicated that MsbA's stabilization occurs alongside two other IMPs, FtsK and LolC (**Figure 2D**). FtsK, one of the longest membrane proteins in *E. coli* (1329 amino acids), belongs to the AAA ATPase family, and LolC is the membrane transport domain of the soluble ABC subunit LolD (Sharma et al., 2021). On the other hand, DgkA, a small diacylglycerol kinase (122 amino acids) displayed destabilization under the same experimental conditions (**Figure 2D**) (Li et al., 2015; Zheng and Jia, 2013). Collectively, these results validate MM-TPP as a straightforward approach to identify ATP binders within a complex population of soluble and integral membrane proteins.

We next applied the MM-TPP workflow to the liver organ, where drug screening for cell surface IMPs is particularly relevant. As anticipated, the total number of proteins identified decreased following heat treatment (**Figure 3A**). Notably, given the absence of detergent, this reduction affected equally soluble proteins and membrane proteins, with the proportion of IMPs remaining stable across temperatures, roughly 48% (**Supplementary Table 1**). We then conducted MM-TPP in the presence of ATP-VO_4 (**Figure 3B**). Similar to findings obtained with the *E. coli* library, the majority of proteins displayed increased thermal stability upon ATP-VO_4 treatment, as indicated by the rightward shift of the datapoints of the plot. Recent studies show that ATP can act as a natural hydrotrope, influencing the global stability of protein populations by interacting with regions sensitive to thermal fluctuations (Ou et al., 2021; Patel et al., 2017).

Important to this study, the GO-term analysis of the significantly stabilized IMPs in the presence of ATP-VO_4 revealed enrichment in functions related to nucleoside-phosphate binding and primary active transport **(Figure 3C)**. Accordingly, inspection of the thermal stability profiles obtained at different temperatures confirmed the particular sensitivity of ABC transporters. Specifically, among the ten ABC transporters identified in the liver library, eight demonstrated significant ATP-VO_4 thermal stabilization under at least one temperature condition **(Table 1** and **Figure 3D)**. Besides ABC transporters, the BCS1L protein exhibited a remarkable ~30-fold increase in stability, which was further enhanced in the presence of AMP-PNP (**Figure 3E** and **Supplementary Figure 2)**. This heightened stability aligns with the recent structural analyses showing that the heptameric BCS1L complex undergoes substantial conformational changes upon binding of this non-hydrolyzable ATP analog (Pan et al., 2023; Tang et al., 2020; Zhan et al., 2024).

A large proportion of IMPs without an ATP-binding annotation were also identified as significantly stabilized in the presence of ATP-VO_4. For example, out of the 178 IMPs above the cut-off significance value, ~ 43% were annotated with GO terms such as nucleic acid/nucleotide, GTP and phosphate binders, among others **(Figure 4A)**. Some IMPs may achieve stability through interactions with ATP-binding proteins, indirectly enhancing their structural stability, as is the case for the LolC/LolD couple above. Conversely, other IMPs may gain stability due to an off-target ligand effect, for example, when metabolized ATP products like ADP, AMP or Pi improve protein stability. This scenario could apply to the purinergic receptor P2RY6, a GPCR responsive to ADP rather than ATP (von Kügelgen and Hoffmann, 2016). This protein displays the highest gain in thermal stability among the other IMPs detected at 56°C (**Supplementary**

File). Similarly, P2RY12, a member of the same GPCR family, showed significant stabilization at all tested temperatures despite its preference for ADP (Entsie et al., 2023; Zhang et al., 2014). In support of this, no such thermal stability gain was obtained when these two receptors were exposed to the ATP analog AMP-PNP (**Figure 4B)**. Conversely, the trimeric ATP-gated cation channel P2RX4 exhibited significant destabilization in the presence of ATP-VO_4 (**Figure 3B)** or AMP-PNP (**Figure 4C**), in agreement with literature reports indicating that members of the P2RX family differ from P2RY due to their preference for ATP (Carnero Corrales et al., 2021; Thompson et al., 2021). Most strikingly, the greatest gain in ATP-induced thermal stability was observed with the FAD-containing monoamine oxidase Mao-B protein at 64°C (**Supplementary Figure 3)**. To identify the potential reason for this major off-target effect, we utilized *AlphaFold3* to model ATP and its derivatives within the FAD-binding pocket of Mao-B (Abramson et al., 2024). Notably, the best fit obtained was for ADP and AMP, with a pLDDT value greater than 90, while ATP generated the lowest pLDDT score (**Figure 4D**). Collectively, these data highlight the ability of MM-TPP to detect the side effects of parent compounds, an important consideration for drug development.

Conclusion

Together, these observations validate the implementation of the peptidisc library in thermal proteome profiling for the detection of membrane protein-ligand interactions at a broad scale level. This approach also enables screening membrane proteomes directly from tissues and organs, ensuring that endogenous protein expression levels, protein-protein interactions, post-translational modifications, and tissue-specific isoforms are preserved, which are often disrupted or altered in traditional cell culture models (Kwasnik et al., 2016; Perez-Perri et al., 2023).

Additionally, MM-TPP's capability to discern stabilization resulting from metabolized products provides additional insights into the dynamics of systems and ligands—an area that remains underexplored in existing TPP literature. While challenges exist, such as maintaining the integrity of physiological pathways that normally occur post-ligand binding, incorporating membrane mimetics in the early stages of drug development offers a promising avenue for understanding how ligands affect cellular systems and how variations in metabolic products can influence drug efficacy and safety.

Methods

Preparation of *Escherichia coli* crude membranes

Wild-type *Escherichia coli* BL21 (DE3) was grown in 1 L of LB medium. After 3 hours, cells were harvested by low-speed centrifugation (6000g, 6 min) and resuspended in Buffer A (50 mM Tris-HCl pH 7.8, 100 mM NaCl, 10% Glycerol) supplemented with 1 mM phenylmethylsulfonyl fluoride (1 mM). Cells were lysed through a microfluidizer (Microfluidics; 3 passes at 15,000 psi at 4 °C). Unbroken cells and large aggregates were removed by low-speed centrifugation (6000g, 6 min). The crude membrane fraction was isolated by ultracentrifugation (100000g, 45 min, 4 °C, Beckman Coulter rotor Ti70). Membranes were resuspended in Buffer A at 5 mg/mL and stored at -80°C for later use.

Expression and purification of His-MsbA for thermal stability assay

Histidine-tagged MsbA (His-MsbA) was expressed, purified, and reconstituted in peptidisc through the on-bead method as described in Angiulli et al. (2020) with slight modifications (Angiulli et al., 2020). Briefly, His-tagged MsbA was produced in *E. coli* BL21(DE3) at 37°C in

1L of LB medium supplemented with 50 µg/mL kanamycin. The inducer IPTG (0.5 mM) was added during the exponential growth phase (OD_{600nm} ~ 0.4). After 3 hours, cells were harvested by low-speed centrifugation (6000g, 6 min) and resuspended in Buffer A (50 mM Tris-HCl pH 7.8, 100 mM NaCl, 10% Glycerol) supplemented with phenylmethylsulfonyl fluoride (1 mM). Cells were lysed through a microfluidizer (Microfluidics; 3 passes at 15,000 psi at 4°C). Unbroken cells and large aggregates were removed by low-speed centrifugation (6000g, 6 min). The crude membrane fraction containing MsbA was isolated by ultracentrifugation (100000g, 45 min, 4°C, Beckman Coulter rotor Ti70). About 2 mg of MsbA-enriched membranes were solubilized with 1% DDM (w/v) for 30 min at 4°C. The detergent solubilized material was ultracentrifuged (180000g, 15 min, 4°C, Beckman Coulter rotor TLA55) to pellet insoluble material. The supernatant was incubated with Ni-NTA (150 µL) resin for 45 min at 4°C on a tabletop rocker. The resin was sedimented through centrifugation (2000g, 1 min) and washed three times with 1.5mL of Buffer A supplemented with 0.02% DDM and 30mM imidazole. After removing the excess buffer, the beads were resuspended in Buffer A containing peptidisc peptide (1 mg/mL). The excess peptide was washed away with Buffer A. The protein was eluted with 600 mM imidazole in Buffer A and the concentration was determined through a Bradford reagent.

Thermal stability assay of His-MsbA with ATP-VO_4

Purified His-MsbA (0.5 mg/mL) in Buffer A supplemented with 5 mM $MgCl_2$ and 0.2 mM orthovanadate (VO_4) was separated into two equal volumes designated as treatment and control samples. To the treatment sample ATP-disodium-trihydrate (ATP) was added to a final concentration of 2mM and an equal volume of ddH2O was administered to the control. Samples

were incubated at room temperature for 10 minutes prior to aliquoting 50 µL into separate 0.2 µL PCR tubes. These aliquots were subjected to temperatures ranging from 45 - 61°C for three minutes followed by ultracentrifugation at 180000g for 15 minutes at 4°C to pellet the unfolded proteins. The supernatants were collected and 10 µL from each sample were analyzed on a 12% SDS-PAGE.

Harvest of *Mus musculus* liver

The C57BL/6 mice were kept in specific pathogen-free conditions and received humane care in compliance with the Canadian Council of Animal Care guidelines, and the animal protocol was approved by the Animal Care Committee of the University of British Columbia. The mouse organs were obtained from female mice. The authors acknowledge that they did not consider the impact of mouse sex at the time of the study design. The mice received standard chow. At the age of 12 weeks, the mice were sacrificed and the liver was excised and placed in vials with ice-cold sterile phosphate-buffered saline (PBS) until processing.

***Mus musculus* liver processing and preparation of crude membranes**

The excised organs were washed several times in ice-cold PBS to remove the blood and then minced and homogenized in ice-cold hypotonic lysis buffer (10 mM Tris–HCl pH 7.4, 30 mM NaCl, and 1 mM EDTA, 1× cocktail protease inhibitor, and 1 mM PMSF) using a tight-fit metal douncer. All subsequent steps were performed at 4 °C or on ice. After adding 10 mM $MgCl_2$ and 50 µg/mL DNase, the suspension was further dounced and incubated for 10 min. The swollen tissue suspension was lysed using a French press (3 passes at 500 PSI). Unbroken cells and nucleus fraction were removed by low-speed centrifugation (1200g for 10 min). The supernatant

was collected and centrifuged at a higher speed (5000g, 10 min) to remove the mitochondrial fraction. The crude membrane fraction was then collected by ultracentrifugation (110000g, 45 min) in a Beckman TLA110 rotor. This membrane pellet was resuspended in 100 µL of 50 mM Tris, pH 7.9, 100 mM NaCl, and 10% glycerol (TSG Buffer) and stored at −80 °C until use.

Preparation of peptidisc membrane protein library

For peptidisc library preparation, ∼2 mg of crude membranes (either *Escherichia coli* or *Mus musculus*) was solubilized in 50 mM Tris, pH 7.9, 25 mM NaCl, and 1% DDM (Solubilization Buffer) for 30 min at 4 °C with gentle shaking. The insoluble material was pelleted by ultracentrifugation (180000g, 15 min). The detergent extract (500 µL) was then reconstituted by mixing it with a 3-fold excess (w/w) peptidisc peptide for 15 min at 4 °C. The sample was rapidly diluted to 15 mL in 50 mM Tris, pH 7.9 and 25 mM NaCl (Buffer A) over a 100 kDa cutoff centrifugal filter. The sample was concentrated (3000g, 10 min) to ∼200 µL. This process was repeated for a total of three rounds of dilution and concentration to deplete DDM to an approximate concentration of 0.008% to complete peptidisc reconstitution. The peptidisc library was immediately used for downstream thermal proteome profiling.

MM-TPP profiling on membrane proteomes

peptidisc membrane protein library was split into two equal aliquots representing the control and treatment samples. Both the treatment and control groups were supplemented with 5 mM $MgCl_2$ and 0.2 mM VO_4. Treatment samples were then exposed to a final concentration of 2 mM ATP while the control received an equal volume of ddH_2O. For experiments with AMP-PNP, 2 mM AMP-PNP was substituted in place of ATP. The samples were incubated for 10 minutes at room

temperature, divided into four aliquots and transferred into 0.2 mL PCR tubes. Each sample was heated in parallel for 3 minutes to their respective temperature (51-64°C). Subsequently, the samples were centrifuged at 180000g for 15 minutes at 4°C and the supernatant was collected for in-solution digestion.

MS sample preparation and LC-MS/MS analysis

Equal volumes of supernatants from the treatment and control groups were treated with 6 M urea at room temperature for 30 min before reduction with 10 mM fresh dithiothreitol (DTT) for 1 h. Alkylation was performed with 20 mM iodoacetamide (IAA) in the dark at room temperature for 30 min, followed by a second round of reduction via 10 mM DTT for 30 min. The urea was diluted to 1 M with Buffer A. Trypsin digestion was performed with an enzyme/protein ratio of 1:100 at room temperature for 24 h. The tryptic peptides were acidified to pH 3 with 10% formic acid and desalted using hand-packed stage tips of C18 resin. The peptides were eluted with 80% acetonitrile and 0.1% formic acid and were dried by vacuum centrifugation. The analysis of tryptic peptides was performed in a NanoLC connected to an Orbitrap Exploris mass spectrometer (Thermo Fisher Scientific) was used for the analysis of all samples. The peptide separation was carried out using a Proxeon EASY nLC 1200 System (Thermo Fisher Scientific) fitted with a custom-made C18 column (15 cm x 150 µm ID) packed with HxSil C18 3 µm Resin 100 Å (Hamilton). A gradient of water/acetonitrile/0.1% formic acid was employed for chromatography. The samples were injected into the column and run for 180 minutes at a flow rate of 0.60 µl/min. The peptide separation began with 1% acetonitrile, increasing to 3% in the first 4 minutes, followed by a linear gradient from 3% to 23% acetonitrile over 86 minutes, then another increase from 24% to 80% acetonitrile over 35 minutes, and finally a 35-minute wash at

80% acetonitrile, and then decreasing to 1% acetonitrile for 10 min and kept 1% acetonitrile for another 10 min. The eluted peptides were ionized using positive nanoelectrospray ionization (NSI) and directly introduced into the mass spectrometer with an ion source temperature set at 250°C and an ion spray voltage of 2.1 kV. Full-scan MS spectra (m/z 350–2000) were captured in Orbitrap Exploris at a resolution of 120,000 (m/z 400). The automatic gain control was set to 1e6 for full FTMS scans and 5e4 for MS/MS scans. Ions with intensities above 1500 counts underwent fragmentation via nanoelectrospray ionization (NSI) in the linear ion trap. The top 15 most intense ions with charge states of ≥ 2 were sequentially isolated and fragmented using normalized collision energy of 30%, activation Q of 0.250, and an activation time of 10 ms. Ions selected for MS/MS were excluded from further selection for 3 seconds. The Orbitrap Exploris mass spectrometer was operated using Thermo XCalibur software.

Data analysis in MaxQuant

Raw mass spectrometric files were analyzed in the MaxQuant environment, version 2.4.1.0. The MS/MS spectra were searched using the Andromeda search engine against the UniProt-mouse protein database (UP000000589, December 2021, 55086 entries) and UniProt-*Escherichia coli* protein database (UP000002032, July 2009, 4156 entries). Precursor mass and fragment mass were set with initial mass tolerances of 20 ppm for both the precursor and fragment ions. The search included variable modifications of asparagine/glutamine deamidation, methionine oxidation, and N-terminal acetylation and a fixed modification of carbamidomethyl cysteine. The maximum number of missed cleavages was set at two, and the maximum modifications/peptide and minimum peptide length were set at six amino acids. The UniProt database was also concatenated with an automatically generated reverse database to estimate the false discovery

rate (FDR) by using a target decoy search. The false discovery rate (FDR) was set at 0.01 for the peptide spectrum match (PSM) and protein identifications. When identified peptides were all shared between two proteins, they were combined and reported as one protein group. For relative quantification, MaxQuant's label-free quantification method, LFQ, was enabled.

Statistical analysis

Each treatment and control sample were collected from three technical replicates. The ProteinGroups.txt output file from MaxQuant was exported into Perseus v1.6.15.0 for downstream analysis. In-house functions of Perseus were used to identify and remove protein groups from the reverse decoy database, those marked as potential contaminants, or those only identified by a post-translational modification site. The remaining intensity, and label-free quantification (LFQ) intensity were $\log_2$ transformed and normalized to the mean peptidisc peptide intensity value. To identify proteins with significant change in thermal stability, a Student's t-test was conducted with a within-groups variance, s0, set to 0.1. The test was applied to data filtered for proteins that had at least three valid LFQ intensities in either the treatment or control group. The remaining undefine intensity values were imputed from a normal distribution with a downshift of 1.8 standard deviations from the total sample mean and a width of 0.3 times the sample standard deviation. To determine significantly stabilized or destabilized as a result of ligand exposure, proteins with a p-value < 0.05 and abundance fold change > 1.8 or < -1.8 were considered as the direct or indirect candidates of ligand-binders. Only proteins with at least two unique peptides were considered for this calculation. To visualise the temperature-dependent peptide intensity data, the smoothed curves were generated using the Piecewise Cubic Hermite Interpolating Polynomial (PCHIP) method. PCHIP interpolation was applied to the mean

intensity values of each experimental group across the temperature gradient. Figures were generated through NumPy, Matplotlib, and Pandas Python coding language.

Ligand binding prediction with AlphaFold3

The web-based AlphaFold server (https://alphafoldserver.com) was utilized to predict ligand binding onto predicted protein structures. Protein peptide sequences were obtained from Uniprot for structure prediction. The resulting output data file was analyzed in Pymol to assess the corresponding B-factor/pLDDT score for each residue interacting with the ligand of interest. The mean pLDDT score from all interacting residues was determined to generate a confidence prediction of ligand binding.

Protein annotation

The protein list obtained from MaxQuant was subjected to a Gene Ontology (GO) term analysis using the UniProtKB database to identify proteins with the GO-term "membrane". Proteins from this group were extracted in FastA format and the Phobius web server ((http://phobius.sbc.su.se/) was utilized to predict the number of transmembrane segments (TMS). Any protein with at least one TMS was classified as an IMP. Protein with no TMS but with the GO annotation "membrane" was classified as a peripherally bound protein, all other proteins were considered as soluble proteins. To assess molecular functions of significantly stabilized IMPs, the Gene Ontology Molecular Function ('GO_MF_Direct/GO_MF_FAT') was used through DAVID Bioinformatics (https://david.ncifcrf.gov/). An EASE score of 0.05 was applied to test for significant GO terms based on a p-value cut-off of 0.05 after Benjamini-Hochberg correction.

The gProfiler g:GOSt tool was utilized to reduce redundancy of significantly enriched terms (https://biit.cs.ut.ee/gprofiler/gost).

Data availability statement

The MS-based proteomics data of this study have been deposited to the ProteomeXchange Consortium via the PRIDE partner repository and are available through the identifier PXD055093.

Acknowledgments

The authors thank Jana Hodasova from the Centre for Comparative Medicine, Animal Care Services at UBC for her help in tissue dissection. This work was supported by the Canadian Institutes of Health Research (CIHR; FDN-154318 to MB and PG20R34019 to FD). RSJ holds a CGS-M scholarship from the Natural Sciences & Engineering Research Council of Canada (NSERC).

References

Abramson J, Adler J, Dunger J, Evans R, Green T, Pritzel A, Ronneberger O, Willmore L, Ballard AJ, Bambrick J, Bodenstein SW, Evans DA, Hung C-C, O'Neill M, Reiman D, Tunyasuvunakool K, Wu Z, Žemgulytė A, Arvaniti E, Beattie C, Bertolli O, Bridgland A, Cherepanov A, Congreve M, Cowen-Rivers AI, Cowie A, Figurnov M, Fuchs FB, Gladman H, Jain R, Khan YA, Low CMR, Perlin K, Potapenko A, Savy P, Singh S, Stecula A, Thillaisundaram A, Tong C, Yakneen S, Zhong ED, Zielinski M, Žídek A, Bapst V, Kohli P, Jaderberg M, Hassabis D, Jumper JM. 2024.

Accurate structure prediction of biomolecular interactions with AlphaFold 3. *Nature* **630**:493–500. doi:10.1038/s41586-024-07487-w

Aebersold R, Mann M. 2016. Mass-spectrometric exploration of proteome structure and function. *Nature* **537**:347–355. doi:10.1038/nature19949

Angiulli G, Dhupar HS, Suzuki H, Wason IS, Duong Van Hoa F, Walz T. 2020. New approach for membrane protein reconstitution into peptidiscs and basis for their adaptability to different proteins. *eLife* **9**:e53530. doi:10.7554/eLife.53530

Antony F, Brough Z, Zhao Z, Duong van Hoa F. 2024. Capture of the Mouse Organ Membrane Proteome Specificity in Peptidisc Libraries. *J Proteome Res* **23**:857–867. doi:10.1021/acs.jproteome.3c00825

Bakheet TM, Doig AJ. 2009. Properties and identification of human protein drug targets. *Bioinformatics* **25**:451–457. doi:10.1093/bioinformatics/btp002

Berlin E, Lizano-Fallas V, Carrasco del Amor A, Fresnedo O, Cristobal S. 2023. Nonionic Surfactants can Modify the Thermal Stability of Globular and Membrane Proteins Interfering with the Thermal Proteome Profiling Principles to Identify Protein Targets. *Anal Chem* **95**:4033–4042. doi:10.1021/acs.analchem.2c04500

Boulos I, Jabbour J, Khoury S, Mikhael N, Tishkova V, Candoni N, Ghadieh HE, Veesler S, Bassim Y, Azar S, Harb F. 2023. Exploring the World of Membrane Proteins: Techniques and Methods for Understanding Structure, Function, and Dynamics. *Molecules* **28**:7176. doi:10.3390/molecules28207176

Carlson ML, Stacey RG, Young JW, Wason IS, Zhao Z, Rattray DG, Scott N, Kerr CH, Babu M, Foster LJ, Duong Van Hoa F. 2019. Profiling the Escherichia coli membrane protein interactome captured in Peptidisc libraries. *eLife* **8**:e46615. doi:10.7554/eLife.46615

Carlson ML, Young JW, Zhao Z, Fabre L, Jun D, Li Jianing, Li Jun, Dhupar HS, Wason I, Mills AT, Beatty JT, Klassen JS, Rouiller I, Duong F. 2018. The Peptidisc, a simple method for stabilizing membrane proteins in detergent-free solution. *eLife* **7**:e34085. doi:10.7554/eLife.34085

Carnero Corrales MA, Zinken S, Konstantinidis G, Rafehi M, Abdelrahman A, Wu Y-W, Janning P, Müller CE, Laraia L, Waldmann H. 2021. Thermal proteome profiling identifies the membrane-bound purinergic receptor P2X4 as a target of the autophagy inhibitor indophagolin. *Cell Chemical Biology* **28**:1750-1757.e5. doi:10.1016/j.chembiol.2021.02.017

Denisov IG, Sligar SG. 2016. Nanodiscs for structural and functional studies of membrane proteins. *Nat Struct Mol Biol* **23**:481–486. doi:10.1038/nsmb.3195

Dörr JM, Koorengevel MC, Schäfer M, Prokofyev AV, Scheidelaar S, van der Cruijsen EAW, Dafforn TR, Baldus M, Killian JA. 2014. Detergent-free isolation, characterization, and functional reconstitution of a tetrameric K+ channel: The power of native nanodiscs. *Proceedings of the National Academy of Sciences* **111**:18607–18612. doi:10.1073/pnas.1416205112

Dunham WH, Mullin M, Gingras A-C. 2012. Affinity-purification coupled to mass spectrometry: Basic principles and strategies. *PROTEOMICS* **12**:1576–1590. doi:10.1002/pmic.201100523

Entsie P, Kang Y, Amoafo EB, Schöneberg T, Liverani E. 2023. The Signaling Pathway of the ADP Receptor P2Y12 in the Immune System: Recent Discoveries and New Challenges. *Int J Mol Sci* **24**:6709. doi:10.3390/ijms24076709

Fagerberg L, Jonasson K, von Heijne G, Uhlén M, Berglund L. 2010. Prediction of the human membrane proteome. *PROTEOMICS* **10**:1141–1149. doi:10.1002/pmic.200900258

Franken H, Mathieson T, Childs D, Sweetman GMA, Werner T, Tögel I, Doce C, Gade S, Bantscheff M, Drewes G, Reinhard FBM, Huber W, Savitski MM. 2015. Thermal proteome profiling for

unbiased identification of direct and indirect drug targets using multiplexed quantitative mass spectrometry. *Nat Protoc* **10**:1567–1593. doi:10.1038/nprot.2015.101

Helbig AO, Heck AJR, Slijper M. 2010. Exploring the membrane proteome—Challenges and analytical strategies. *Journal of Proteomics* **73**:868–878. doi:10.1016/j.jprot.2010.01.005

Huber KVM, Olek KM, Müller AC, Tan CSH, Bennett KL, Colinge J, Superti-Furga G. 2015. Proteome-wide drug and metabolite interaction mapping by thermal-stability profiling. *Nat Methods* **12**:1055–1057. doi:10.1038/nmeth.3590

Jandu RS, Yu H, Zhao Z, Le HT, Kim S, Huan T, Hoa FD van. 2024. Capture of endogenous lipids in peptidiscs and effect on protein stability and activity. *iScience* **27**. doi:10.1016/j.isci.2024.109382

Kalxdorf M, Günthner I, Becher I, Kurzawa N, Knecht S, Savitski MM, Eberl HC, Bantscheff M. 2021. Cell surface thermal proteome profiling tracks perturbations and drug targets on the plasma membrane. *Nat Methods* **18**:84–91. doi:10.1038/s41592-020-01022-1

Kawatani M, Osada H. 2014. Affinity-based target identification for bioactive small molecules. *Med Chem Commun* **5**:277–287. doi:10.1039/C3MD00276D

Kwasnik A, Tonry C, Ardle AM, Butt AQ, Inzitari R, Pennington SR. 2016. Proteomes, Their Compositions and Their Sources In: Mirzaei H, Carrasco M, editors. Modern Proteomics – Sample Preparation, Analysis and Practical Applications, Advances in Experimental Medicine and Biology. Cham: Springer International Publishing. pp. 3–21. doi:10.1007/978-3-319-41448-5_1

Li D, Stansfeld PJ, Sansom MSP, Keogh A, Vogeley L, Howe N, Lyons JA, Aragao D, Fromme P, Fromme R, Basu S, Grotjohann I, Kupitz C, Rendek K, Weierstall U, Zatsepin NA, Cherezov V, Liu W, Bandaru S, English NJ, Gati C, Barty A, Yefanov O, Chapman HN, Diederichs K, Messerschmidt M, Boutet S, Williams GJ, Marvin Seibert M, Caffrey M. 2015. Ternary

structure reveals mechanism of a membrane diacylglycerol kinase. *Nat Commun* **6**:10140. doi:10.1038/ncomms10140

Li J, Xu H, West GM, Jones LH. 2016. Label-free technologies for target identification and validation. *Med Chem Commun* **7**:769–777. doi:10.1039/C6MD00045B

Lomenick B, Hao R, Jonai N, Chin RM, Aghajan M, Warburton S, Wang J, Wu RP, Gomez F, Loo JA, Wohlschlegel JA, Vondriska TM, Pelletier J, Herschman HR, Clardy J, Clarke CF, Huang J. 2009. Target identification using drug affinity responsive target stability (DARTS). *Proc Natl Acad Sci U S A* **106**:21984–21989. doi:10.1073/pnas.0910040106

Lyu J, Liu C, Zhang T, Schrecke S, Elam NP, Packianathan C, Hochberg GKA, Russell D, Zhao M, Laganowsky A. 2022. Structural basis for lipid and copper regulation of the ABC transporter MsbA. *Nat Commun* **13**:7291. doi:10.1038/s41467-022-34905-2

Mateus A, Kurzawa N, Becher I, Sridharan S, Helm D, Stein F, Typas A, Savitski MM. 2020. Thermal proteome profiling for interrogating protein interactions. *Mol Syst Biol* **16**:e9232. doi:10.15252/msb.20199232

Molina DM, Jafari R, Ignatushchenko M, Seki T, Larsson EA, Dan C, Sreekumar L, Cao Y, Nordlund P. 2013. Monitoring Drug Target Engagement in Cells and Tissues Using the Cellular Thermal Shift Assay. *Science* **341**:84–87. doi:10.1126/science.1233606

Ou X, Lao Y, Xu J, Wutthinitikornkit Y, Shi R, Chen X, Li J. 2021. ATP Can Efficiently Stabilize Protein through a Unique Mechanism. *JACS Au* **1**:1766–1777. doi:10.1021/jacsau.1c00316

Pai MY, Lomenick B, Hwang H, Schiestl R, McBride W, Loo JA, Huang J. 2015. Drug Affinity Responsive Target Stability (DARTS) for Small Molecule Target Identification. *Methods Mol Biol* **1263**:287–298. doi:10.1007/978-1-4939-2269-7_22

Pan Y, Zhan J, Jiang Y, Xia D, Scheuring S. 2023. A concerted ATPase cycle of the protein transporter AAA-ATPase Bcs1. *Nat Commun* **14**:6369. doi:10.1038/s41467-023-41806-5

Patel A, Malinovska L, Saha S, Wang J, Alberti S, Krishnan Y, Hyman AA. 2017. ATP as a biological hydrotrope. *Science* **356**:753–756. doi:10.1126/science.aaf6846

Perez-Perri JI, Ferring-Appel D, Huppertz I, Schwarzl T, Sahadevan S, Stein F, Rettel M, Galy B, Hentze MW. 2023. The RNA-binding protein landscapes differ between mammalian organs and cultured cells. *Nat Commun* **14**:2074. doi:10.1038/s41467-023-37494-w

Reinhard FBM, Eberhard D, Werner T, Franken H, Childs D, Doce C, Savitski MF, Huber W, Bantscheff M, Savitski MM, Drewes G. 2015. Thermal proteome profiling monitors ligand interactions with cellular membrane proteins. *Nat Methods* **12**:1129–1131. doi:10.1038/nmeth.3652

Santos R, Ursu O, Gaulton A, Bento AP, Donadi RS, Bologa CG, Karlsson A, Al-Lazikani B, Hersey A, Oprea TI, Overington JP. 2017. A comprehensive map of molecular drug targets. *Nat Rev Drug Discov* **16**:19–34. doi:10.1038/nrd.2016.230

Savitski MM, Reinhard FBM, Franken H, Werner T, Savitski MF, Eberhard D, Molina DM, Jafari R, Dovega RB, Klaeger S, Kuster B, Nordlund P, Bantscheff M, Drewes G. 2014. Tracking cancer drugs in living cells by thermal profiling of the proteome. *Science* **346**:1255784. doi:10.1126/science.1255784

Sharma S, Zhou R, Wan L, Feng S, Song K, Xu C, Li Y, Liao M. 2021. Mechanism of LolCDE as a molecular extruder of bacterial triacylated lipoproteins. *Nat Commun* **12**:4687. doi:10.1038/s41467-021-24965-1

Tang WK, Borgnia MJ, Hsu AL, Esser L, Fox T, de Val N, Xia D. 2020. Structures of AAA protein translocase Bcs1 suggest translocation mechanism of a folded protein. *Nat Struct Mol Biol* **27**:202–209. doi:10.1038/s41594-020-0373-0

Thompson RJ, Sayers I, Kuokkanen K, Hall IP. 2021. Purinergic Receptors in the Airways: Potential Therapeutic Targets for Asthma? *Front Allergy* **2**. doi:10.3389/falgy.2021.677677

Urner LH, Liko I, Pagel K, Haag R, Robinson CV. 2022. Non-ionic hybrid detergents for protein delipidation. *Biochimica et Biophysica Acta (BBA) - Biomembranes* **1864**:183958. doi:10.1016/j.bbamem.2022.183958

von Kügelgen I, Hoffmann K. 2016. Pharmacology and structure of P2Y receptors. *Neuropharmacology*, Special Issue: Purines in Neurodegeneration and Neuroregeneration **104**:50–61. doi:10.1016/j.neuropharm.2015.10.030

Yang Z, Wang C, Zhou Q, An J, Hildebrandt E, Aleksandrov LA, Kappes JC, DeLucas LJ, Riordan JR, Urbatsch IL, Hunt JF, Brouillette CG. 2014. Membrane protein stability can be compromised by detergent interactions with the extramembranous soluble domains. *Protein Sci* **23**:769–789. doi:10.1002/pro.2460

Ye Y, Li K, Ma Y, Zhang X, Li Y, Yu T, Wang Y, Ye M. 2023. The Introduction of Detergents in Thermal Proteome Profiling Requires Lowering the Applied Temperatures for Efficient Target Protein Identification. *Molecules* **28**:4859. doi:10.3390/molecules28124859

Young JW. 2023. Recent advances in membrane mimetics for membrane protein research. *Biochem Soc Trans* **51**:1405–1416. doi:10.1042/BST20230164

Zhan J, Zeher A, Huang R, Tang WK, Jenkins LM, Xia D. 2024. Conformations of Bcs1L undergoing ATP hydrolysis suggest a concerted translocation mechanism for folded iron-sulfur protein substrate. *Nat Commun* **15**:4655. doi:10.1038/s41467-024-49029-y

Zhang J, Zhang K, Gao Z-G, Paoletta S, Zhang D, Han GW, Li T, Ma L, Zhang W, Müller CE, Yang H, Jiang H, Cherezov V, Katritch V, Jacobson KA, Stevens RC, Wu B, Zhao Q. 2014. Agonist-bound structure of the human P2Y12 receptor. *Nature* **509**:119–122. doi:10.1038/nature13288

Zhang X, Ruan C, Zhu H, Li K, Zhang W, Wang K, Hu L, Ye M. 2020. A Simplified Thermal Proteome Profiling Approach to Screen Protein Targets of a Ligand. *PROTEOMICS* **20**:1900372. doi:10.1002/pmic.201900372

Zhao Z, Khurana A, Antony F, Young JW, Hewton KG, Brough Z, Zhong T, Parker SJ, Duong van Hoa F. 2023. A Peptidisc-Based Survey of the Plasma Membrane Proteome of a Mammalian Cell. *Mol Cell Proteomics* **22**:100588. doi:10.1016/j.mcpro.2023.100588

Zheng J, Jia Z. 2013. Tiny enzyme uses context to succeed. *Nature* **497**:445–446. doi:10.1038/nature12245

Figures

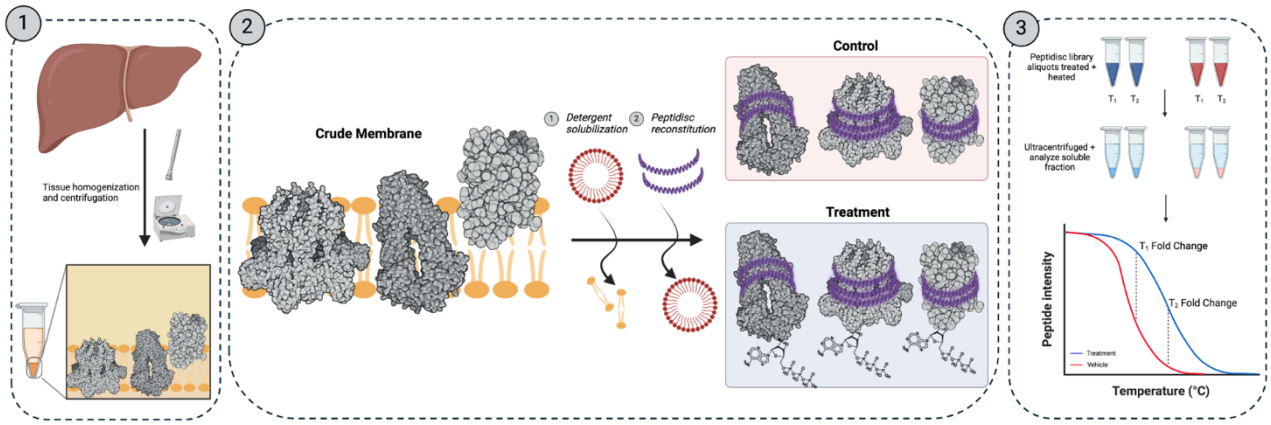

Figure 1: The Membrane Mimetic-Thermal Proteome Profiling (MM-TPP) experimental workflow. 1) Crude membranes are prepared from the liver organ. **2)** Integral membrane proteins (IMPs) are solubilized with detergent and reconstituted in the Peptidisc library. The water-soluble library is exposed to the ligand of interest (treatment) or corresponding vehicle (control)**. 3)** Protein samples are heated at specific temperatures to induce precipitation, followed by ultracentrifugation. The soluble fraction is analyzed by mass spectrometry to detect changes in protein abundances between treatment and control sample

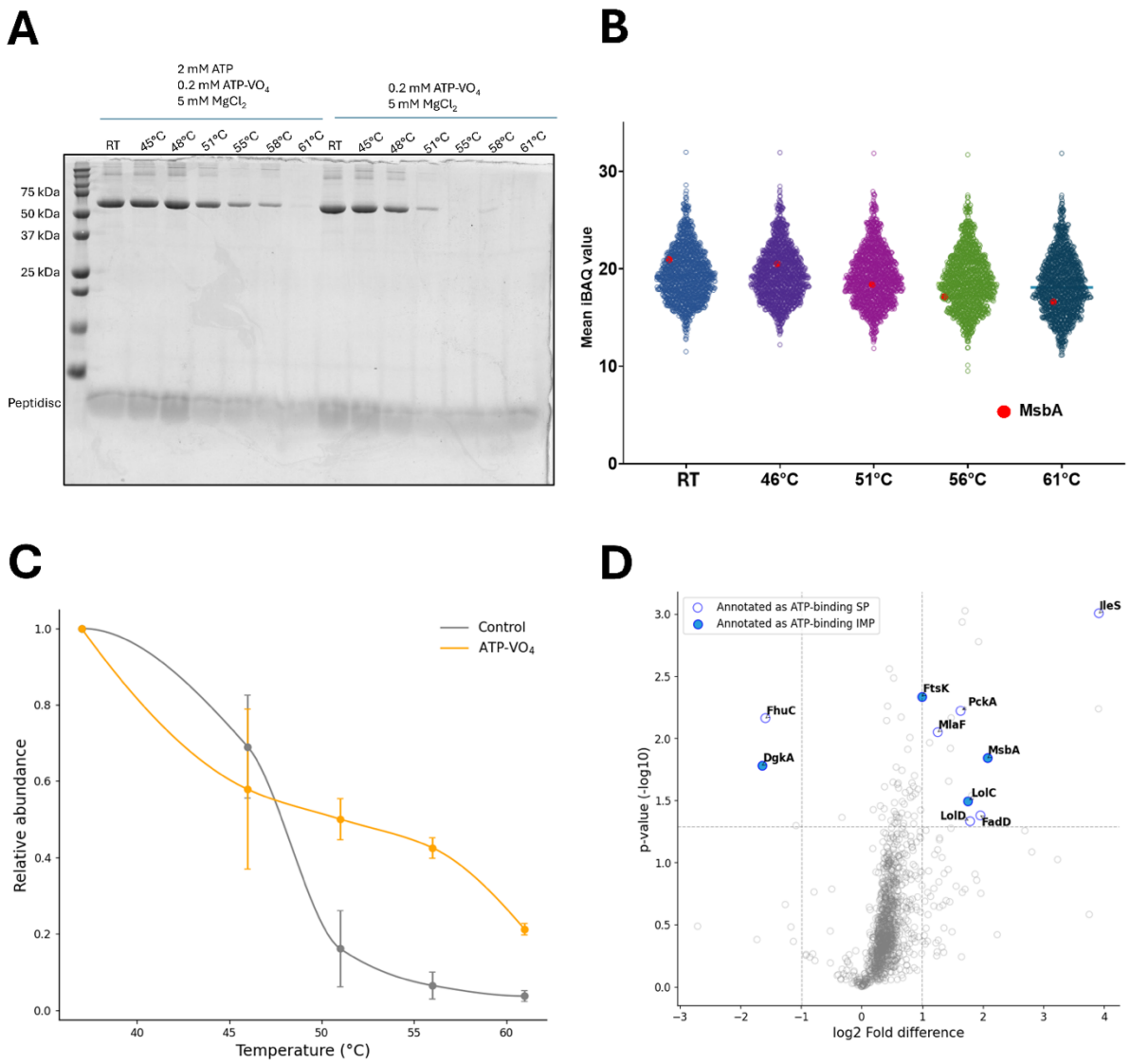

Figure 2: MM-TPP of integral membrane proteins (IMPs) prepared from *E. coli*. (**A**) Stability of purified MsbA in Peptidisc in the presence of the indicated ligands. Samples are heat treated and centrifuged before analysis by 12% SDS-PAGE and Coomassie blue staining. (**B**) Grouped scatterplot representation of mean IBAQ value obtained for all identified proteins in the *E. coli* library at the indicated temperatures. The location of MsbA on the plot is shown as a red dot. The mean value is obtained from three replicates of the temperature exposure assay (n = 3). (**C**) Relative abundance of MsbA based on the peptide intensities obtained across temperatures in

the presence of ATP-VO_4 (orange) compared to a control sample (gray). Data is a mean ± standard deviation from triplicate assays (n = 3). **(D)** Volcano plot analysis of stabilized and destabilized proteins following ATP-VO_4 exposure at 61°C. A fold difference significance cut off of +2 and -2 with a p-value cutoff of $p \leq 0.05$ is applied. Hollow blue dots indicate ATP-binding soluble proteins (SP) and solid blue dots indicate ATP-binding IMPs. Data represents the mean from three replicates (n = 3).

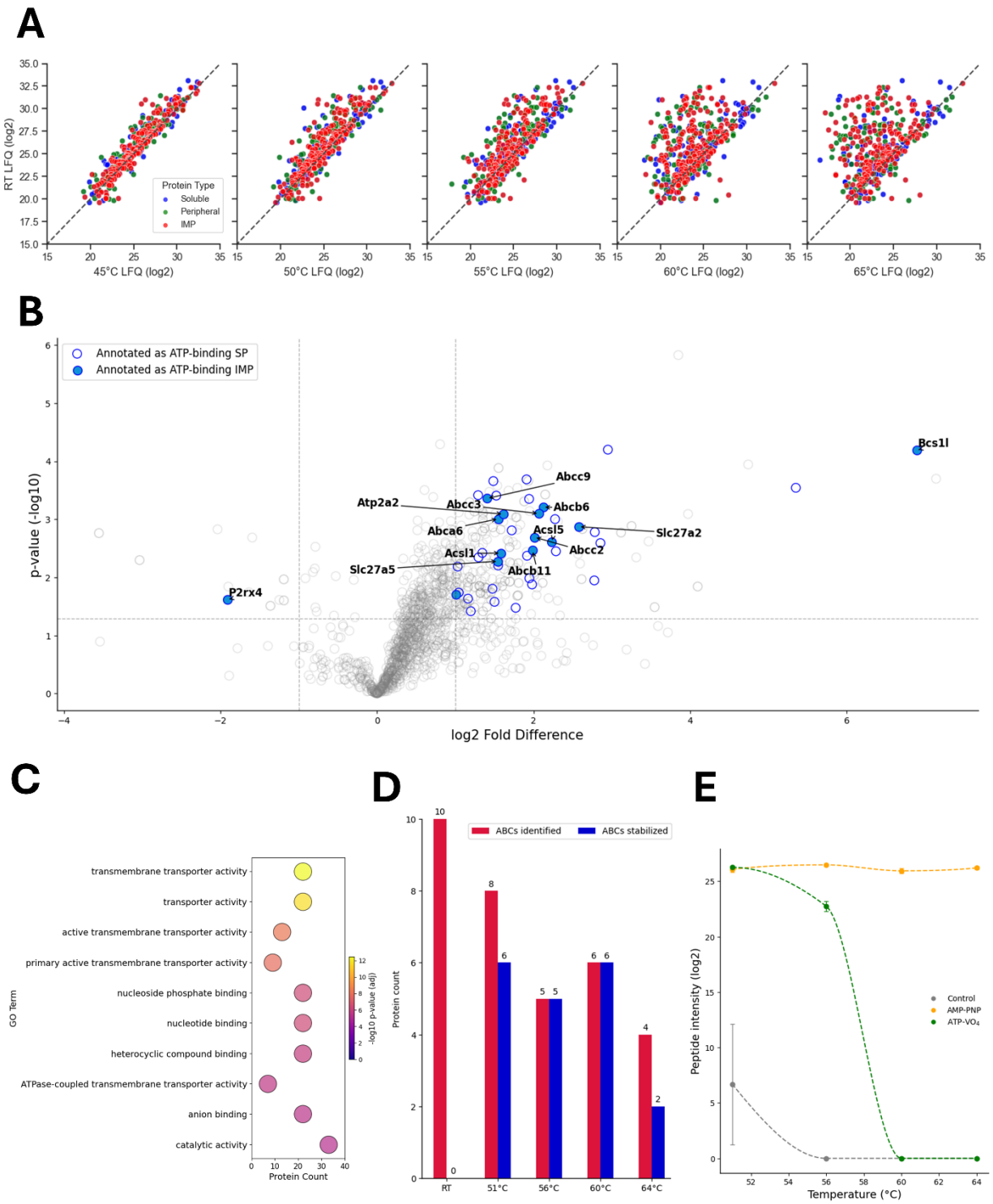

Figure 3: MM-TPP of integral membrane proteins (IMPs) prepared from the mouse liver organ. (**A**) Global protein intensities derived from label-free quantification (LFQ) values of

peptidisc-reconstituted liver extract. The plot displays soluble proteins, peripherally bound and IMPs identified at the indicated temperatures compared to room temperature (RT). The dashed line is the identical value line. (**B**) Volcano plot of stabilized and destabilized proteins at 51°C based on a fold difference cutoff of > 2 or < -2 and p-value of ≤ 0.05. The ATP-binding soluble proteins (SP) are represented as hollow blue circles, and the ATP-binding IMPs are represented as solid blue circles. The mean value is obtained from three replicates at the temperature exposure assay (n = 3). (**C**) GO-term enrichment analysis of molecular functions of stabilized IMPs identified in B. The presented top 10 significant terms are based on adjusted p-value (FDR = 5% after Benjamini-Hochberg correction) (**D**) Number of ATP-binding cassette (ABC) transporters identified and stabilized by ATP-VO_4 at the indicated temperatures. (**E**) Peptide intensities of BCS1L in the presence of ATP-VO_4 (green), AMP-PNP (orange), and vehicle control (gray) across the temperature range. Data is a mean ± standard deviation from three replicates (n = 3).

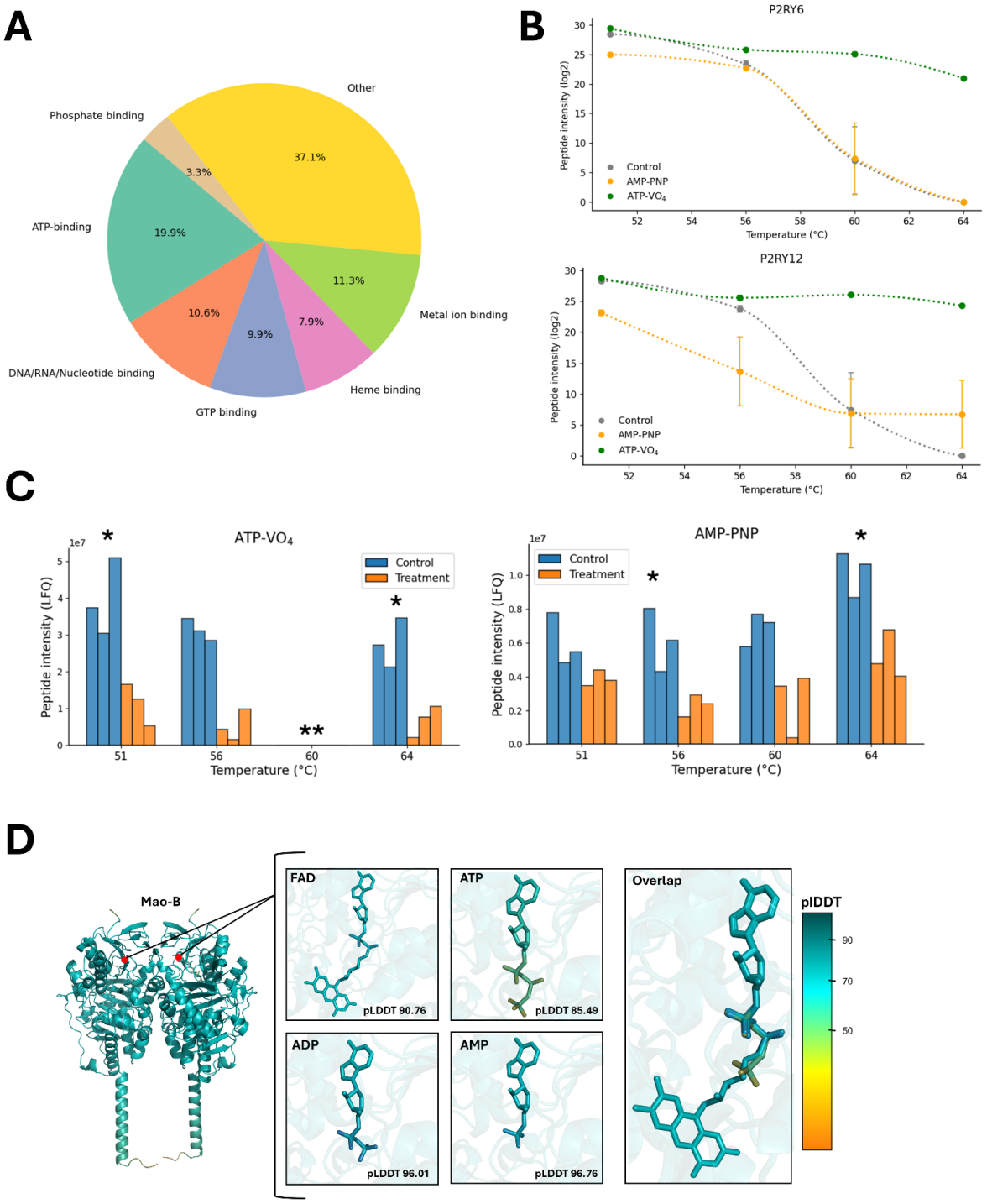

Figure 4: Off-target ATP ligand effect. (**A**) GO-term analysis of molecular functions and distribution for all IMPs significantly stabilized at all temperatures tested with the mouse liver

library (n = 178). (**B**) Peptide intensity variations of P2RY6 and P2RY12 over the temperature range with AMP-PNP (orange), ATP-VO_4 (green), or none (gray). Data is a mean ± standard deviation from three replicates (n = 3). **(C)** Peptide intensity variations of P2RX4 at the indicated temperature in the presence of ATP-VO4 (left panel) or AMP-PNP (right panel). Data from treatment samples (orange) and control samples (blue) is from triplicates (n = 3). * Represents p-value ≤ 0.05. **Protein not detected. (**D**) Structural model of homodimeric Mao-B with the predicted binding of FAD, ATP, ADP, and AMP ligands within the FAD binding pocket, indicated as red dots. Each ligand is presented individually in the FAD binding pocket or as an all-ligand overlap generated by *AlphaFold3*. The respective Predicted Local Distance Difference Test (pLDDT) score for each ligand is shown, with higher scores representing more favourable ligand fitting. The colour gradient represents a high pLDDT score as blue and a low pLDDT score as orange.

Table 1: ATP-binding cassette transporters detected in the mouse liver peptidisc library. At least two unique peptides were detected per protein at each temperature. Stabilization was defined using a fold change > 2 between treatment and control samples, with a significance set at $p \leq 0.05$, calculated from triplicate samples (n = 3).

Uniprot-ID	Protein Name	Full protein name	Stabilized temperatures (°C)
Q8K441	ABCA6	ATP-binding cassette sub-family A member 6	51, 56, 60, 64
J3QNY6	ABCB11	ATP-binding cassette, sub-family B (MDR/TAP), member 11	51, 56, 60
Q9DC29	ABCB6	ATP-binding cassette sub-family B (MDR/TAP), member 6	51
Q8VI47	ABCC2	ATP-binding cassette sub-family C (CFTR/MRP), member 2	51, 56, 60
A0A0R4J015	ABCC3	ABC-type glutathione-S-conjugate transporter (CFTR/MRP)	51, 60
P70170	ABCC9	ATP-binding cassette sub-family C member 9 (Sulfonylurea receptor 2)	51, 56, 60
S4R2E1	ABCG2	ATP-binding cassette sub-family G member 2) (Urate exporter)	56, 60, 64
Q99PE8	ABCG5	ATP-binding cassette sub-family G member 5 (Sterolin-1)	51

Supplementary Figures

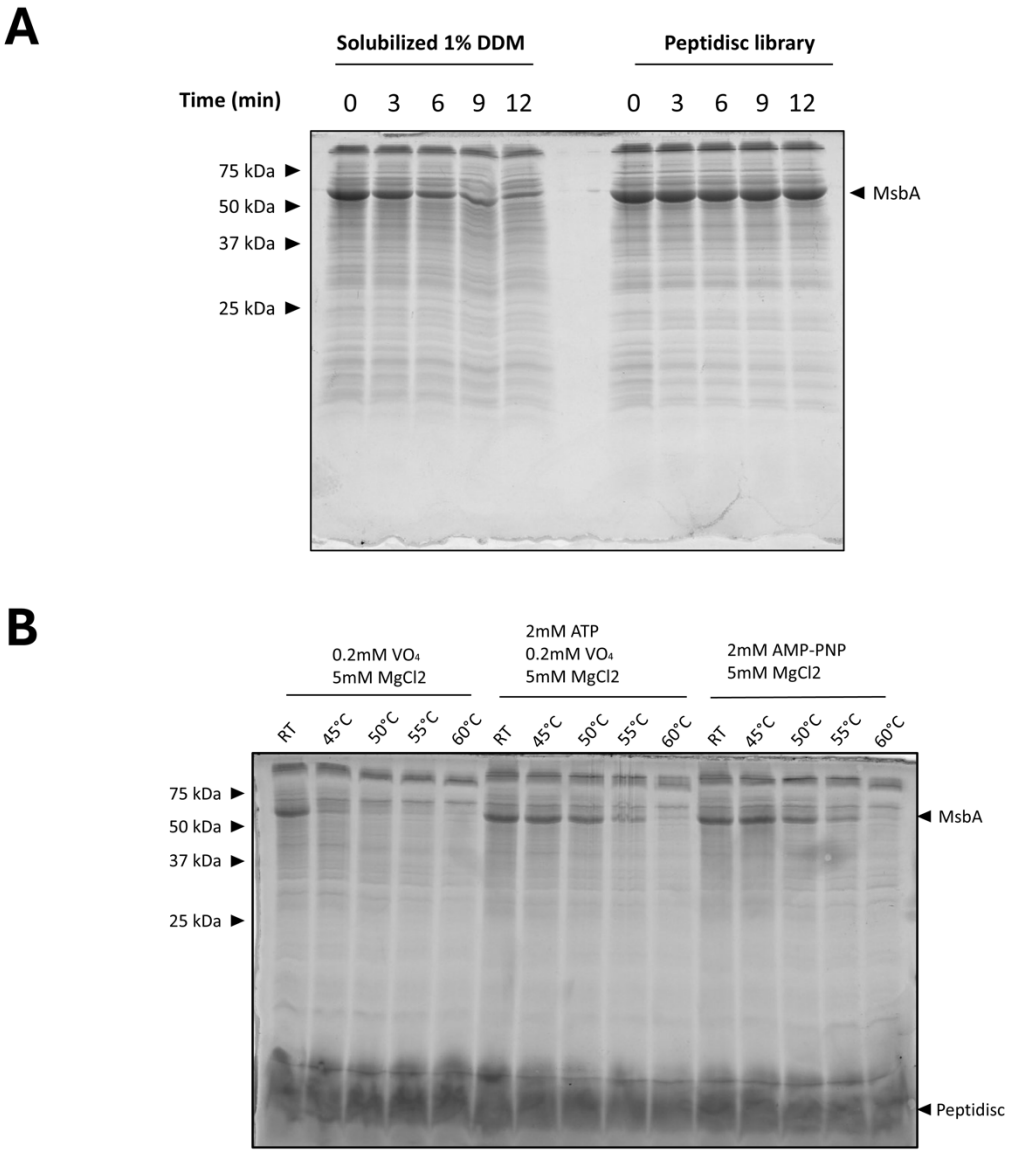

Supplementary Figure 1: Thermal stability of MsbA in detergent or with ligands. (**A**) The *E. coli* membrane fraction enriched for MsbA was solubilized with 1% DDM or reconstituted in Peptidisc. The detergent extract and Peptidisc library were incubated at 45°C for the indicated times. After centrifugation, the supernatants were analyzed on 15% SDS-PAGE and visualized

with Coomassie blue staining. (**B**) The Peptidisc library prepared in (A) was incubated with ATP-VO_4 or AMP-PNP at the indicated temperature. Supernatants were analyzed on 15% SDS-PAGE and visualized with Coomassie blue staining.

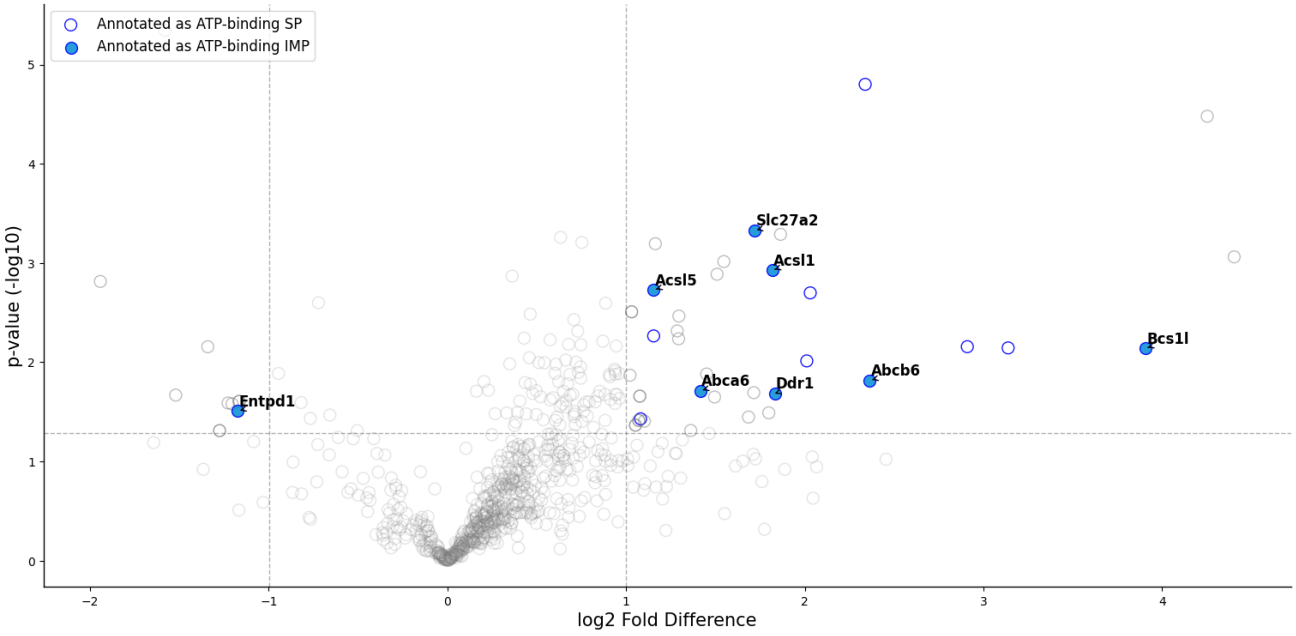

Supplementary Figure 2: Volcano plot of stabilized and destabilized proteins at 51°C in the presence of AMP-PNP. Soluble proteins (SP) annotated as ATP-binding proteins are presented as hollow blue circles, and IMPs annotated as ATP-binding are presented as solid blue circles. The mean value is obtained from three replicates at the temperature exposure assay (n = 3).

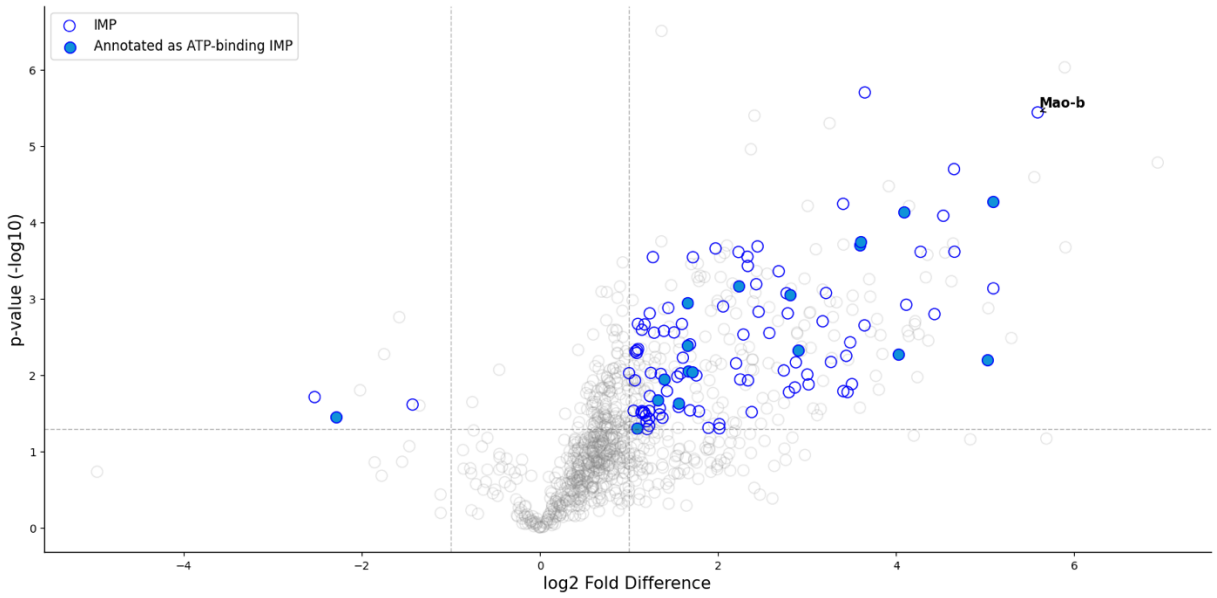

Supplementary Figure 3: Volcano plot of stabilized and destabilized proteins at 64°C in the presence of ATP-VO_4. Stabilized and destabilized IMPs are represented by hollow blue circles and IMPs annotated as ATP-binding are represented by solid blue circles with label on Mao-B. The mean value is obtained from three replicates at the temperature exposure assay (n = 3).

Supplementary Table 1: Number of proteins identified in the mouse liver peptidisc library at the indicated temperature to assess loss of IMPs compared to global protein abundance. At least two unique peptides were identified for each protein (n = 2).

Temperature	Total protein	Total IMP
Room temperature	998 ± 2	470 ± 3 (47%)
45°C	892 ± 11	425 ± 1 (48%)
50°C	810 ± 16	385 ± 7 (48%)
55°C	734 ± 46	354 ± 22 (48%)
60°C	566 ± 33	276 ± 11 (49%)
65°C	524 ± 4	264 ± 3 (50%)